Available online at www.sciencedirect.com
ScienceDirect
Journal of Hazardous Materials 150 (2008) 136–145
Journal of Hazardous Materials
www.elsevier.com/locate/jhazmat

High temperature ablation of kaolinite layered silicate/phenolic resin/asbestos cloth nanocomposite

Ahmad Reza Bahramian [a], Mehrdad Kokabi [a,*], Mohammad Hossein Navid Famili [a], Mohammad Hossein Beheshty [b]

[a] *Polymer Engineering Group, Chemical Engineering Department, Faculty of Engineering, Tarbiat Modares University, PO Box 14115-143, Tehran, Iran*
[b] *Department of Composites, Iran Polymer and Petrochemical Institute, PO Box 14965-115, Tehran, Iran*

Received 22 November 2006; received in revised form 8 April 2007; accepted 19 April 2007
Available online 4 May 2007

Abstract

The successful return of re-entry space vehicle, which is subjected to severe aerodynamic heating, is largely accompanied by some provisions to reduce the heat transfer to the structure. Heat shield is the best protection means which undergoes physical, chemical, and mostly endothermal transformations.

The objective of this work is to investigate the ablating, charring, and thermal degradation behaviour of heat shield resol-type phenolic resin/kaolinite/asbestos cloth nanocomposite by oxyacetylene flame test with an external heat flux of 8×10^9 W/m^2 and 3000 K hot gas temperature and thermal analyzer techniques.

Kinetic parameters of thermal degradation and temperature distribution at the back surface of the nanocomposite heat shield were determined and compared with that of composite counterpart.

Keywords: Ablative; Nanocomposite; Layered structure; Composite; Kaolinite

1. Introduction

Despite of the great deal of research performed on the thermal degradation of polymeric structure as a complex phenomenon, many aspects are still unclear [1–7]. The thermal degradation covers a wide field of important processes, such as the development of heat resistant, thermal stabilization, ablation and the characterization of high temperature structure for aircraft and aerospace usage [3].

In the ablation process, the high heat fluxes are dissipated by the material through a series of endothermic processes. That finally leads to the loss and the consumption of the material itself [5]. The working process of an ablative heat shield can be briefly summarized as follows; the convective heat that reaches to the vehicle surface is balanced by surface radiation, phase transitions, and chemical reactions. Moreover, part of the incoming convective heat flux is blocked by the outcoming flow of hot gases that result from the degradative processes [5,8].

Thermal protection via ablation is achieved through a self-regulating heat and mass transfer process involving an insulator with low thermal conductivity and the sacrificial pyrolysis and concomitant formation of a tough refractory char on the insulator surface. Above the decomposition temperature, the insulator produces pyrolysis gases in the reaction zone and degrades to a char layer at higher temperatures. The majority of mass loss occurs in the reaction zone. The presence of the char layer regulates penetration of heat from the surface and produces a steep temperature gradient [9].

Recent advances in polymer layered silicate nanocomposites encourage the examination of this unique class of evolving materials as potential ablatives [9]. Polymer layered silicate nanocomposites show excellent potential as ablative materials because upon pyrolysis, the organic–inorganic nanostructure reinforcing the polymer can be converted into a uniform ceramic char, which may lead to significantly increased resistance to oxidation and mechanical erosion in comparison with composite ablative materials [9–12].

* Corresponding author. Tel.: +98 21 8801 1001; fax: +98 21 8800 6544.
E-mail address: mehrir@modares.ac.ir (M. Kokabi).

0304-3894/$ – see front matter © 2007 Elsevier B.V. All rights reserved.
doi:10.1016/j.jhazmat.2007.04.104

Nomenclature

A	Frequency factor of composite (s^{-1})
A_c	Frequency factor for char formation (s^{-1})
A_g	Frequency factor for gas formation (s^{-1})
C1	Primary char
C2	Secondary char
$d_{001}\|_K$	Basal distance of initial kaolinite (°A)
$d_{001}\|_{KDC}$	Basal distance of kaolinite DMSO complex (°A)
E	Activation energy of composite thermal degradation ($J\,mol^{-1}$)
E_c	Activation energy for char formation ($J\,mol^{-1}$)
E_g	Activation energy for gas formation ($J\,mol^{-1}$)
$f(\alpha)$	Conversion functional relationship
G	Mass rate of gaseous products of composite thermodecomposition ($kg\,s^{-1}\,m^{-2}$)
G1	Primary gas
G2	Secondary gas
I^*	Reactive intermediate
k	Rate constant (s^{-1})
k_c	Rate constant for char formation (s^{-1})
k_g	Rate constant for gas formation (s^{-1})
k_p	Rate constant for polymer formation (s^{-1})
m	Weight of sample (kg)
m_0	Initial weight of the sample (kg)
m_f	Final weight of the sample (kg)
m_p	Specific pyrolysis mass flow rate ($kg\,m^{-2}\,s^{-1}$)
n	Degree of thermal degradation reaction
P	Composite
R	Universal gas constant ($J\,kg^{-1}\,mol^{-1}\,K^{-1}$)
t	Time (s)
T	Absolute temperature (K)
V	Volatile
y_c	Yield of charring
α	Degree of thermal degradation
β	Heating rate ($K\,s^{-1}$)

Kaolinite is an aluminosilicate with the ideal composition $Al_2Si_2O_5(OH)_4$. Moreover, kaolinite is a 1:1 dioctahedral clay mineral whose structure is composed of interstratified $AlO_2(OH)_4$ octahedral sheets and SiO_4 tetrahedral sheets [13,14]. Consequently, the interlayer space is unsymmetrical, which is not found in the other layered materials [13]. Van der Waals bonds between the aluminol and Si–O groups link adjacent lamella to each other, and frequently make the intercalation processes difficult [15].

The successful intercalation agents decrease the electrostatic attraction between the lamellae by causing an increase in the dielectric constant when the compounds penetrate between the layers [16]. The kind of guest species intercalated between the layers of kaolinite is limited due to hydrogen bonding between hydrogen groups of $AlO_2(OH)_4$ octahedral sheets and SiO_4 tetrahedral sheets. Only a limited number of polar guest species, such as dimethylsulfoxide (DMSO) can directly be intercalated [17,18].

In this work, the ablative performance and thermal decomposition of phenolic resin/kaolinite/asbestos cloth ablative nanocomposites as a heat shield are examined in comparison with asbestos phenolic resin/cloth composite.

2. Kinetic models of thermal degradation

It is worth bearing in mind that all of the mechanisms and equation derivations used in this section were comprehensively recorded in our previous work [19].

Thermal degradation simplified in three processes: heating, thermal decomposition, and ignition of the gaseous decomposed products in air [19–21].

Pyrolysis gases mix and react with air in the combustion zone above the surface releasing heat and producing carbon dioxide, water and incomplete combustion products, such as carbon monoxide. The basic thermal degradation mechanism leading to volatile fuel generation in char forming polymers has been described as a generalized chemical bond scission process consisting of primary and secondary decomposition events. The primary decomposition step is side chain scission of the polymer to form intermediates. The primary char decomposes by dehydrogenation to form the secondary gas and thermally stable secondary char [21].

A simple solution for the mass loss history of a polymeric material allows estimation of the generation rate under isothermal and nonisothermal heating, and can be verified using standard laboratory thermogravimetric techniques. By considering some assumptions, the process of thermal degradation will be reduced and simplified. The following assumptions are considered [19,21,22];

A: The breaking of primary chemical bonds in the polymer is the rate limiting step.
B: The reactive intermediate is in dynamic equilibrium with the parent polymer.
C: Thermal degradation of primary char to secondary char and gas is slow compared to the formation of the primary char.
D: The oxidative environment in the pyrolysis zone of a thermal degradation solid polymer is anaerobic.
E: All of the chemical reactions are of first order.
F: Assumptions A–E lead to a simplified mass loss model as follows [15,19,21]:

$$\frac{m(t)}{m_0} = 1 - \left[\frac{k_g}{k_g + k_c}\right]\left\{1 - \exp(-k_p t)\right\} \tag{1}$$

Eq. (1) shows that as $t \to \infty$, the residual mass approaches an equilibrium value at constant temperature given by [19–21]:

$$\frac{m(\infty)}{m_0} = \left[\frac{k_c}{k_g + k_c}\right] = y_c \tag{2}$$

Assuming Arrhenius forms for k_g, ($k_g = A_g \exp(-E_g/RT)$) and k_c, ($k_c = A_c \exp(-E_c/RT)$) in Eq. (2):

$$\ln\left[\frac{1 - y_c}{y_c}\right] = \ln\left[\frac{A_g}{A_c}\right] - \left[\frac{E_g - E_c}{R}\right]\frac{1}{T} \tag{3}$$

Substituting Eq. (2) into Eq. (1) yields the final results for the isothermal mass loss history in terms of the rate constant for thermolysis of primary chemical bonds, k_p as:

$$\frac{m(t)}{m_0} = y_c + (1 - y_c)\exp(-k_p t) \tag{4}$$

For a constant heating rate, $\beta = dT/dt$, the independent variable, i.e., $k_p t$, in Eq. (4) can be transformed from time to the dimensionless variable. The exact solution of Eq. (4) for the fractional mass as a function of temperature at constant heating rate is [19,21]:

$$\frac{m(T)}{m_0} = y_c + (1 - y_c)\exp\left[-\frac{A}{\beta}(T - T_0)e^{-E/RT}\right] \tag{5}$$

The fractional mass loss rate during a linear temperature program is obtained by differentiating Eq. (5) with respect to time. No simple solution is possible when $y_c = y_c(T)$, so we make the approximation that the char yield is constant and not a function of temperature, thus with $y_c = \mu$, we obtain [19,21]:

$$\frac{-1}{m_0}\frac{dm}{dt} = (1 - \mu)k_p(T)\left(1 + \frac{(T - T_0)E}{RT^2}\right) \times \exp\left[\frac{-(T - T_0)k_p(T)}{\beta}\right] \tag{6}$$

The rate of weight loss in thermogravimetric analysis is dependent on temperature, and can be expressed as [19,23–25]:

$$\frac{d\alpha}{dt} = kf(\alpha) \tag{7}$$

The rate constant could be described as an Arrhenius form as:

$$k = A\exp\left(\frac{-E}{RT}\right) \tag{8}$$

As mentioned earlier, according to the assumptions made, all of the chemical reactions are first order, but the mass loss of composite and nanocomposite system are of nth order. Integrating Eq. (8) with respect to temperature and using the phase boundary reaction method for textile polymeric system($f(\alpha) = (1 - \alpha)^n$), the final result could be expressed as:

$$\frac{d\alpha/dt}{(1 - \alpha)^n} = A\exp\left(-\frac{E}{RT}\right) \tag{9}$$

3. Experimental

3.1. Materials

A resol type phenolic resin (IL800/2) supplied by Resitan company, with the properties given in reference [19], was used as the polymeric matrix.

Asbestos cloth (Grade AAA) was added as reinforcing to the polymeric matrix. Properties of asbestos cloth are given in [19].

The kaolinite sample employed in this work was separated from Semirom natural clay. Dimethylsulfoxide (DMSO), ammonium hydroxide (NH_4OH) and ethyl alcohol were high-purity lab grade from Merck and used as received.

3.2. Preparation of kaolinite –DMSO complex

To obtain the intercalated samples the natural clay (kaolinite) was firstly disaggregated, weighed, and dispersed in a dilute ammonium hydroxide solution (100 ml NH_4OH and 4000 ml of water) for 24 h. Then, left for 3–4 h and subsequently, the dispersion was decanted and separated from the rest. This procedure was repeated until a relative large quantity of aqueous solution containing fine clay was obtained.

The solvent was removed by drying at 70 °C for 24 h. For washing with distilled water, a kaolinite-water solution (60 mg of clay in 1 cm^3 of distilled water) was made. This solution was also dried at 100 °C.

To modify the kaolinite, approximately 100 g of the clay fraction was transferred to a 5000 ml round-bottom flask and suspended in 4000 ml of DMSO (95 v/v % DMSO: water). The suspension was stirred at 60 °C for 192 h and then centrifuged at 4000 rpm to recover the solids.

To remove the residual DMSO, the resultant material (kaolinite-DMSO complex) was dried at 40 °C for 120 h and subsequently characterized [15,16].

3.3. Nanocomposite preparation

In this work, the combination of solution and in situ intercalation is employed for nanocomposite sample preparation, as follows:

Ethyl alcohol is used to disperse the layered silicates which are intercalated with DMSO and at the same time to dissolve the phenolic resin. To stack the layers the crystallite is delaminated in ethyl alcohol. This will occur due to the weak van der Waals force. Phenolic resin then can be adsorbed onto the delaminated individual layer. However, upon ethyl alcohol removal the layers can reassemble to reform the stack with phenolic chains sandwich in between, forming a well order intercalated nanocomposites.

Asbestos cloth impregnated by phenolic resin/layered silicate intercalated. The sample was precured at 120 °C for 10 min, and then cured at 160 °C and 3 bar for an hour in autoclave. After curing, the composite was postcured for 0.5 h at 150 °C. Therefore, due to ethyl alcohol removal and phenolic resin polymerisation, the nanocomposite samples were formed.

The final sample is a flat panel by dimensions of $6 \times 100 \times 100$ mm with a sandwich structure, formed from 4 mm layers nanocomposite and 2 mm layer of aluminum substrate. For oxyacetylene flame test, the nickel-chrome thermocouple was placed on the back of the sample. This is shown in Fig. 1. The characteristic of samples are given in Table 1.

3.4. Nanocomposite characterization

The structure of the polymer layered silicate nanocomposites has traditionally been elucidated using X-ray diffraction (XRD) and transmission electron microscopy (TEM) [12]. The most straightforward is XRD. The sample preparation is relatively easy and the X-ray analysis can be performed within a few hours [9–13].

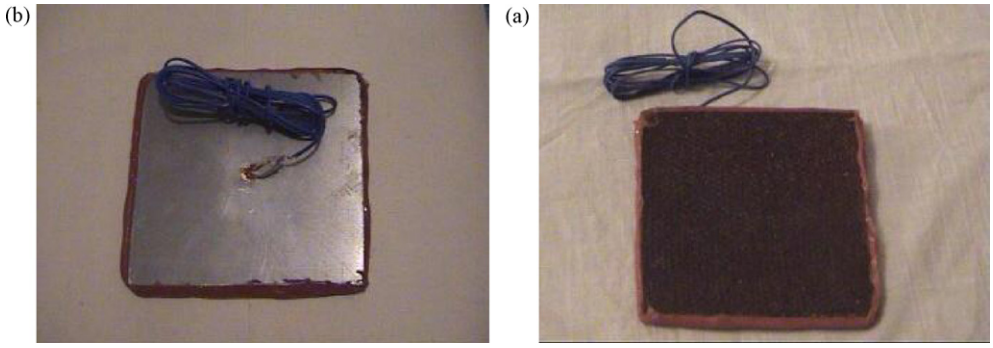

Fig. 1. The sample for oxyacetylene flame test, top (a) and back (b) surface of the sample.

To analyze the specimen, XRD a Miniflex diffractometer using Cu Kα radiation with a dwell time of 1°/min, in the 2θ Bragg–Brentano geometry was employed.

X-ray fluorescence (XRF) measurements were also carried out in a PW 2400, Philips spectrometer.

Transmission electron microscopy is a useful complement to XRD. TEM gives a direct measure of the spatial distribution of the layers, but it requires substantial skills in specimen preparation and analysis [12,13]. Because of the presence of asbestos cloth reinforcement (around 50 wt.%) in our samples, the TEM test cannot give useful information. Instead of TEM, scanning electron microscopy (SEM) and surface scattering of atomic tracing testes were used to confirm the nanocomposite formation.

Scanning electron microscopy (SEM) studies were carried out using a CanScan FE microscope with a field emission gun operating at 20 kV acceleration voltages. The samples were coated with a 2–3 nm gold/palladium films using a Denton Magnetron Sputter coater system.

STA 625, Polymer Laboratories (TG and TGA) was employed to evaluate the thermal performance of the insulation material samples.

To evaluate the thermal behaviour and ablation performance of the ablative material insulators, the oxyacetylene flame test is performed according to ASTM-E-285–80. This test can create hot gas with 3400 K and 9×10^6 W/m K heat flux. Hot combustion gases are directed along the normal to the specimen. The results of the test are useful to show the thermal behaviour of ablative materials. This test method covers the screening of ablative materials to determine the relative thermal insulation effectiveness when tested as a flat panel in an environment of a steady flow of hot gas provided by an oxyacetylene burner.

Cone calorimetry was employed on an Atlas CONE2 according to ASTM E 1354 at a heat flux of 80 kW/m^2, which is a normal irradiance level for the evaluation of the flammability, using a cone shaped heater.

Table 1
The characteristics of the samples

Sample	Component	m_{clay}/m_{resin}	W_{resin}	W_{clay}	$W_{asbestos}$
Composite	Asbestos cloth/phenolic resin composite	0.00	0.50	0.00	0.50
NKA1	Asbestos cloth/phenolic resin/kaolinite nanocomposite	0.06	0.47	0.03	0.50
NKA2	Asbestos cloth/phenolic resin/kaolinite nanocomposite	0.10	0.44	0.04	0.52
NKA3	Asbestos cloth/phenolic resin/kaolinite nanocomposite	0.14	0.42	0.06	0.52

4. Results and discussion

4.1. Composition and morphology

The chemical composition of natural kaolinite and modified kaolinite (kaolinite-DMSO complex) was detected by XRF to determine the impurity of initial kaolinite and the evaluation of purification process, Table 2.

If SiO_2 and Al_2O_3 are assumed as net kaolinite, the percent of purity increases from 80.32% in natural kaolinite to 95.7% in modified kaolinite with DMSO. XRF cannot detect the organic part of the modified kaolinite, i.e., DMSO. It is about 25.121%.

It is observed that the more impurities (especially Na_2O) were removed after the chemical treatments.

Fig. 2 compares the XRD spectra of the modified kaolinite (kaolinite/DMSO complex) with initial kaolinite. The analysis of the 001 d-spacing and 2θ are reported in Table 3. In modified kaolinite, basal reflection (d_{001}) peak was shifted to lower

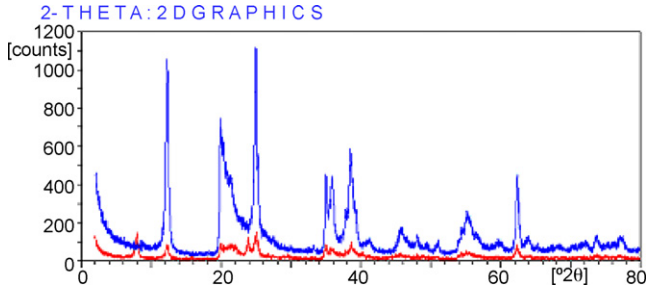

Fig. 2. X-ray diffraction patterns of initial (upper curve) and modified (lower curve) kaolinite.

Table 2
The chemical composition of the initial and modified kaolinite obtained by XRF

	Chemical composition (mass %)	Initial kaolinite	Modified kaolinite	Modified kaolinite (normalized)
Kaolinite	SiO_2	41.763	38.292	51.102
	Al_2O_3	38.569	33.365	44.527
Common impurity	MgO	0.411	0.257	0.342
	SO_3	0.115	–	–
	Cl	0.116	–	–
	K_2O	0.268	0.239	0.319
	CaO	0.745	0.312	0.416
	TiO_2	1.513	1.437	1.917
	Fe_2O_3	1.391	0.871	1.163
	Zr	0.029	0.026	0.034
Major impurity	Na_2O	15.08	0.079	0.105
	Total	100	74.932	100
	Non-detectable material (organic part, i.e., DMSO)	–	25.121	–
	Purity (%)	80.32	–	95.629

Table 3
Identification of the phase, basal distance and interlayer expansion

Phase	2θ (°)	$\Delta 2\theta$ (°)	d_{001}(°A)	Δd[a](°A)
Kaolinite	12.3	0.0	7.1	0.0
Kaolinite-DMSO complex	7.9	−4.4	11.2	4.1

[a] $\Delta d = d_{001}|-d_{001}|_K$.

angle and decreased strongly. Variation in the interplanar spacing was determined by subtracting the basal lattice value of the intercalated kaolinite from the basal lattice value of raw kaolinite.

The basal space of modified kaolinite was 11.2°A at $2\theta = 7.9°$, which represents an expansion of 4.1°A, related to the basal space of the raw kaolinite (7.1°A at $2\theta = 12.3°$).

Fig. 3. compares the XRD patterns of nanocomposite (6 wt.%) and composite and shows any significant difference. As observed there is no trace of kaolinite peaks in the nanocomposite XRD pattern. It means the nanocomposite has an exfoliated morphology.

As mentioned the atomic tracing (SEM surface scattering) was employed as a complement technique for XRD analysis to evaluate the exfoliation and dispersion of layered silicate in resin, Fig. 4. This figure clearly shows the Si atoms are well uniformly distributed in nanocomposite along a solid line.

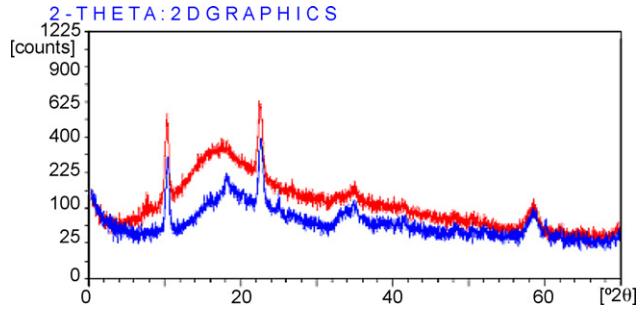

Fig. 3. X-ray diffraction patterns of nanocomposite (6 wt.%) (lower curve) and composite (upper curve).

4.2. Thermal behaviour

Fig. 5 shows the TG analysis of the initial and modified kaolinite. This figure indicates the initial loss weight of DMSO is started at a temperature of 150 °C and completed at around 300 °C. The total mass loss is approximately less than 29% which its major part is attributed to DMSO.

Fig. 6 shows a TGA thermogram of weight loss as a function of temperature for phenolic/asbestos composite and NKA1, NKA2, and NKA3 nanocomposites (defined in Table 1) in an air atmosphere. In general, major weight losses are observed on the range of ∼300–500 °C for all the specimens. Evidently, the thermal decomposition of the phenolic/asbestos-kaolinite nanocomposites shifts slightly toward the higher temperature range comparing with that of phenolic/asbestos composite, and confirms the enhancement of thermal stability of nanocomposite. After ∼600 °C, mainly the inorganic residue is remained.

Linear dependency of the $\ln((d\alpha/dt)/(1-\alpha)^n)$ versus the reciprocal of temperature can be obtained by choosing a certain

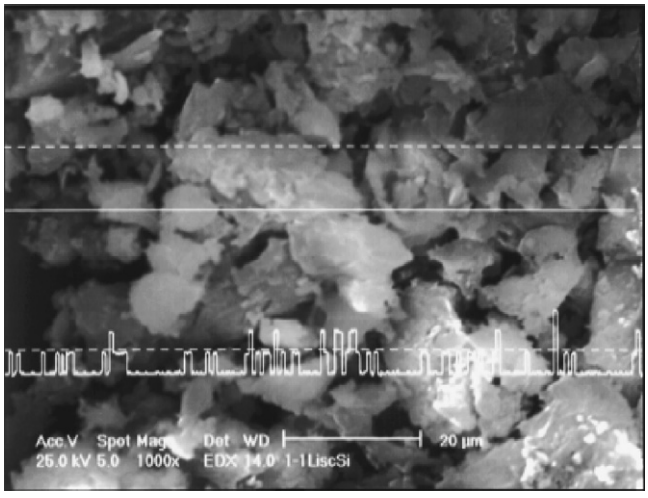

Fig. 4. Surface scattering of Si atoms in intercalated layered silicate/phenolic resin nanocomposite.

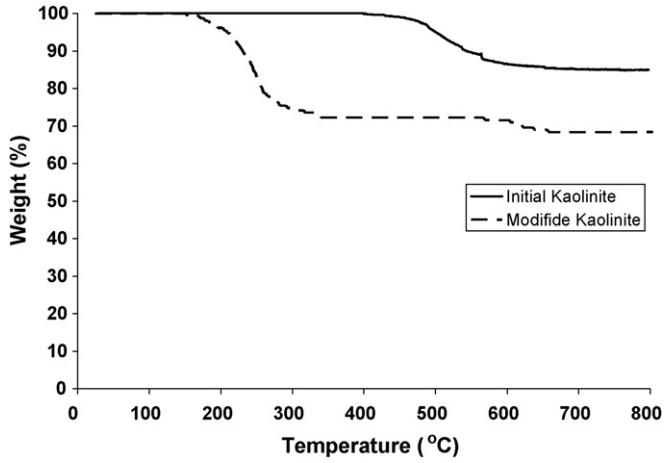

Fig. 5. The TGA curves of initial and modified kaolinite.

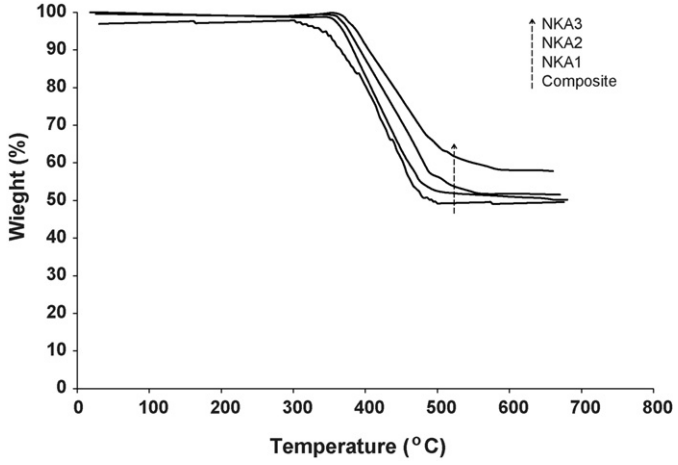

Fig. 6. The TGA curves of composite and nanocomposite samples.

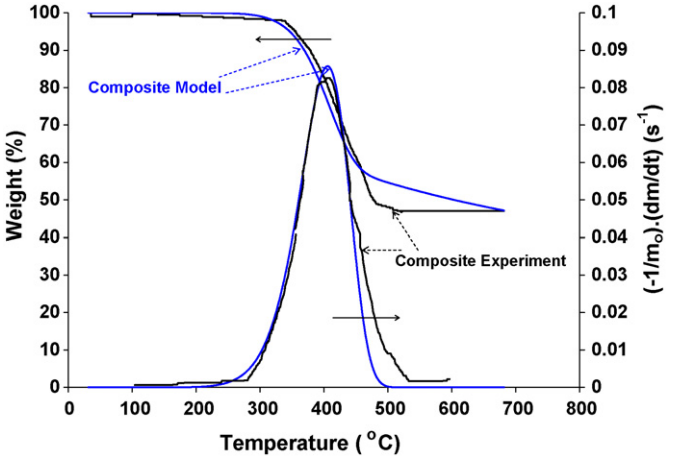

Fig. 7. The thermogravimetric curves of asbestos/phenolic composite at 10 °C/min in air, in comparison with the model.

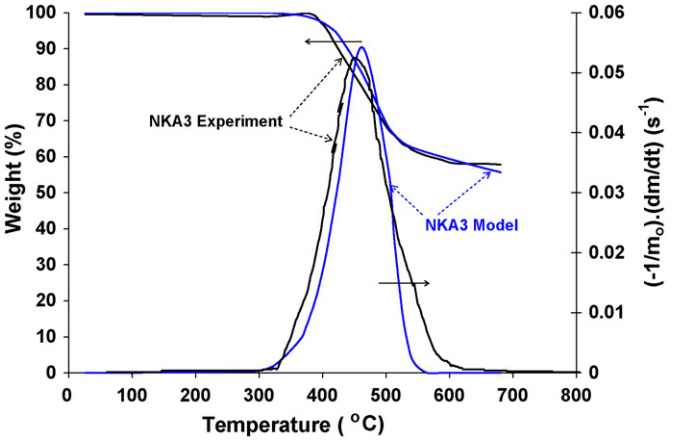

Fig. 8. The thermogravimetric curves of NKA3 at 10 °C/min in air, in comparison with the model.

n. From this correlation, and Eq. (9), the activation energies, E, frequency factor, A, and degree of thermal degradation, n, are evaluated by linear regression analysis of the data points.

The relative rate constants for volatile and char formation are obtained by plotting Eq. (3). Thus, a plot of $\ln[(1-y_c)/y_c]$ versus $1/T$ has a slope proportional to the difference in activation energies for volatile and char formation and an intercept which is the natural logarithm of the ratio of the frequencies factors.

The thermal degradation kinetic parameters of the samples are given in Table 4. It can be seen that the activation energy of composite is nearly three orders of magnitude larger than the activation energy of net phenolic resin. This is due to asbestos cloth chemical reactions and its interaction with resin. Similar data were reported by the other researchers, (for asbestos cloth phenolic resin composite, [19,23] and net phenolic resin, [19,24,25]).

Table 4
The kinetic parameters of the samples

Kinetic parameter	Unit	Phenolic resin (in nitrogen) [19]	Composite (in nitrogen) [19]	Composite (in air)	NKA3 (in air)
Activation energy, E	J/mol	1.43×10^5	1.75×10^8	9.57×10^7	12×10^7
The difference in activation energy for volatile and char formation, $E_g - E_c$	J/mol	4.1×10^4	3.92×10^7	1.01×10^7	1.3×10^7
Frequency factor, A	s^{-1}	3×10^9	1.26×10^{10}	8.82×10^4	8.9×10^4
The fraction of frequency factor for volatile and char formation, Ag/Ac	–	13	46.5	4	4.1
Degree of thermal degradation reaction, n	–	1	6.5	1.7	1.7

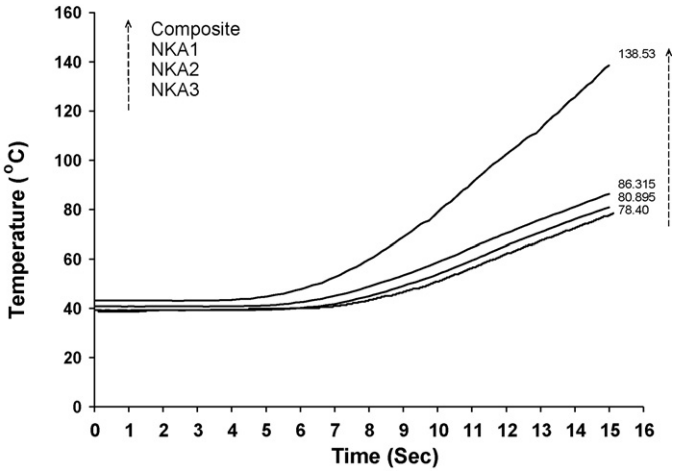

Fig. 9. Temperature distribution of back surface of the asbestos/phenolic composite and NKA1,NKA2, and NKA3 nanocomposites; which measured in oxyacetylene flame test.

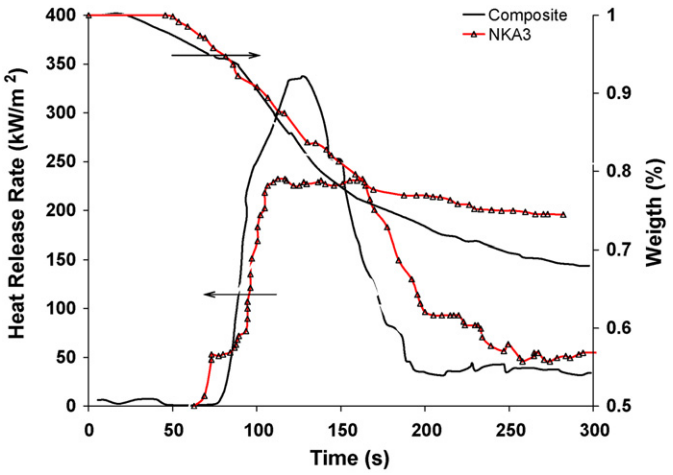

Fig. 10. Comparison of the heat release rate (HRR) and the mass loss plot for phenolic asbestos cloth composite and phenolic asbestos cloth kaolinite nanocomposite (NKA3) at 80 kWm^{-2} heat flux.

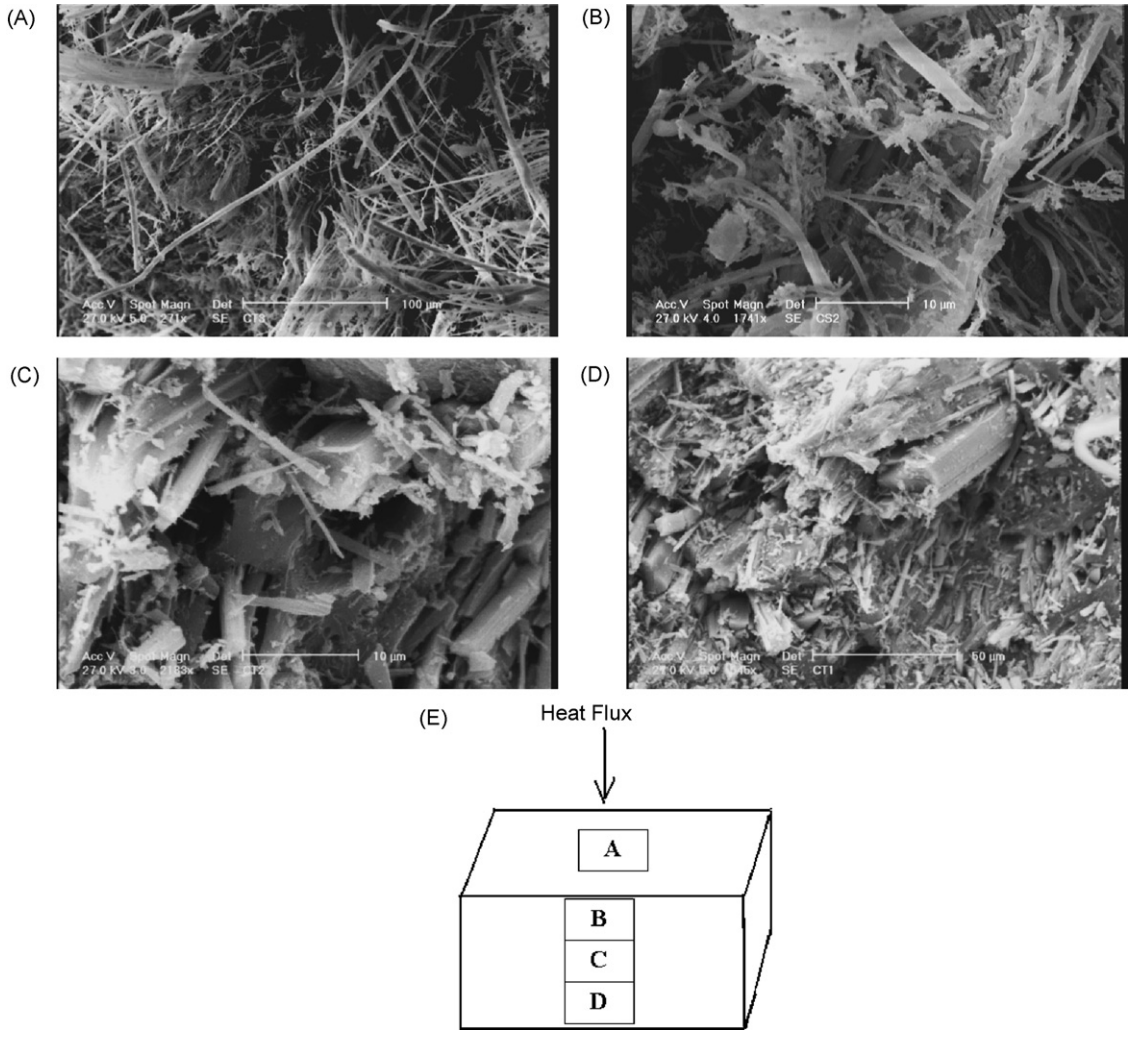

Fig. 11. Scanning electron micrographs of asbestos-phenolic composite after cone calorimetery test. (A) Top surface and (B), (C), and (D) lateral surface, and (E) illustrating the heat flux direction.

Figs. 7 and 8 show TGA and DTA weight loss experimental points of asbestos/phenolic composite and NKA3 nanocomposite at 10 K/min in air, compared with the theoretical curves generated by Eqs. (5) and (6), respectively. As shown in these figures, due to a good agreement between experimental data and model predictions, all of the calculated kinetic parameters are reliable.

4.3. Ablation performance

Fig. 9 shows the temperature distribution at the back surface of NKA1, NKA2, and NKA3 nanocomposites in comparison with asbestos/phenolic composite. These temperature distributions were measured experimentally by oxyacetylene flame test. Test duration is 15 s and external conventional heat flux is 9×10^6 W/m K. At the end of the test, the back surface temperature of a 4 mm thickness NKA3, NKA2, NKA1 and asbestos/phenolic composite are 78.4, 80.89, 86.315, and 138.53 °C, respectively. It shows that the back surface temperature of NKA3 nanocomposites, for example, is 43.4% lower than composite.

The heat release rate (HRR) and mass loss plots for asbestos cloth/phenolic composite and NKA3 nanocomposite at 80 kW/m^2 heat flux are shown in Fig. 10. This figure shows that composite and nanocomposite behave thermally similar until 100 s of the flame test. After that, by increasing the surface temperature to 1000 °C, rate of mass loss and HRR of nanocomposite decrease. It is concluded that the NKA3 nanocomposite has a 35% lower HRR and 22% lower mass loss than the asbestos cloth/phenolic composite.

Figs. 11 and 12 show scanning electron micrographs of the asbestos-phenolic composite and NKA3 nanocomposite ablative sample after cone calorimetry test, respectively. These figures are illustrating top surface (surface of char region), lateral surfaces, and heat flux direction. The characteristic of ablation regions, virgin material, porous reaction zone and dense char layer are apparent in all of the samples. Therefore, the microstructural of nanocomposite char implies that increasing

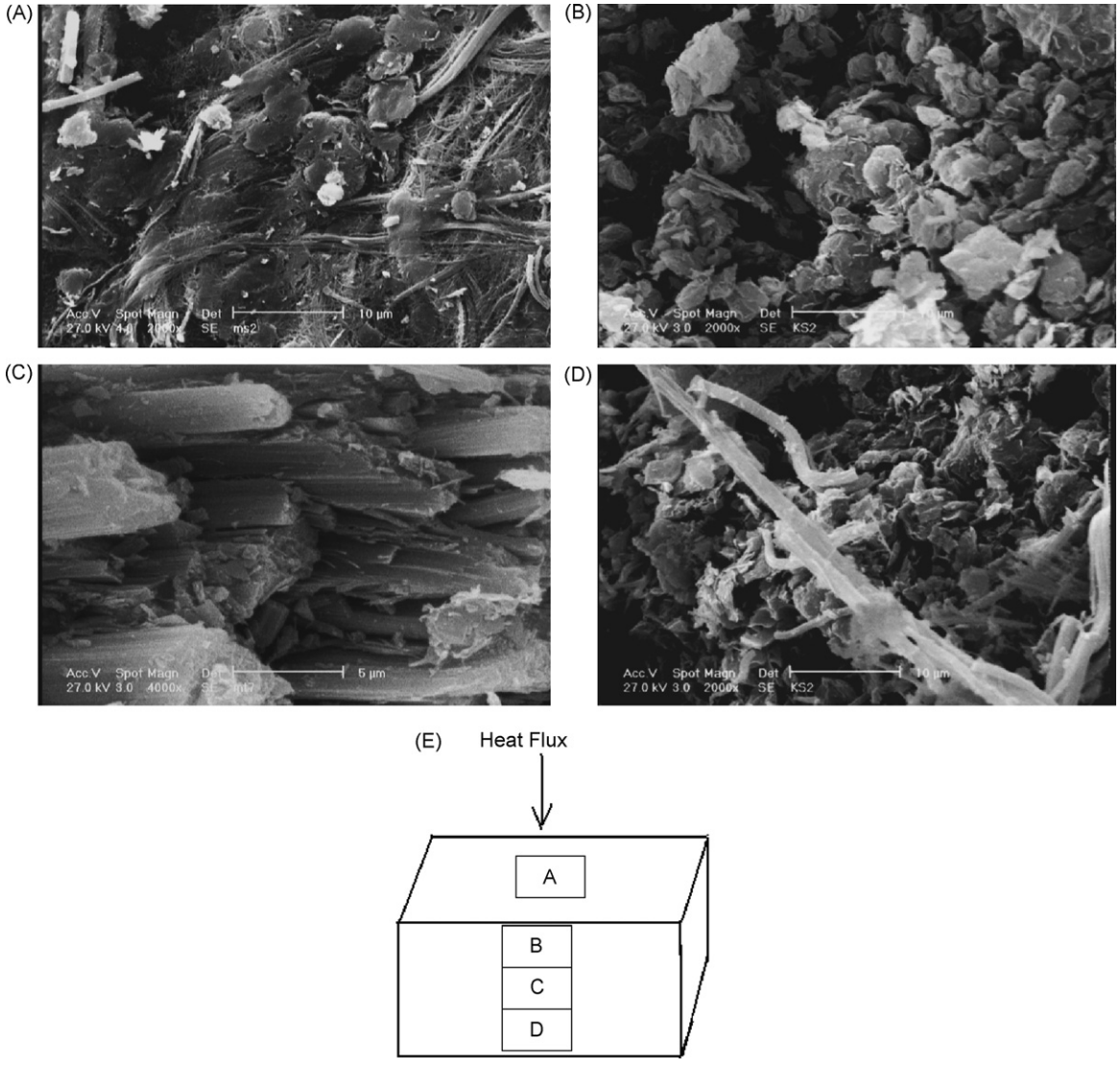

Fig. 12. Scanning electron micrographs of NKA3 nanocomposite after cone calorimetery test. (A) Top surface and (B), (C), and (D) lateral surface, and (E) illustrating the heat flux direction.

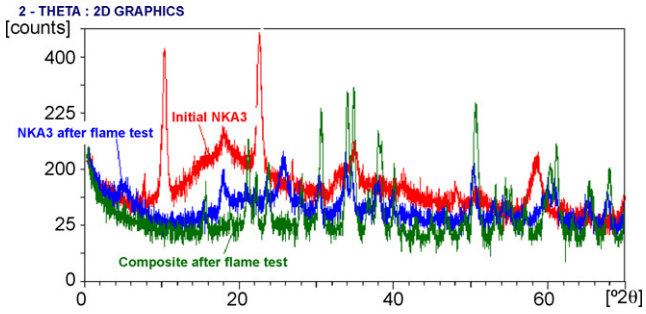

Fig. 13. X-ray diffraction patterns of initial NKA3, NKA3 after flame test, and composite after flame test.

clay content results in a tougher char. In these chars, a nanoscopic packed platy morphology is observed, Fig. 12B.

In general, the spatially uniform arrangement of the silicate layers on an ultra-fine nanometer level facilitates the formation of a spatially uniform inorganic char. This clay dense char causes the higher performance of nanocomposites at high temperature by forming the secondary ceramic layer heat shield on the top surface of the ablative nanocomposites.

Fig. 13. shows the XRD patterns of initial NKA3, NKA3 after flame test, and composite sample after flame test. This analysis shows that the mineral composition of composite due to flame test changes from clinochrysotile ($Mg_3Si_2O_5(OH)_4$ to forsterite (Mg_2SiO_4). NKA3 nanocomposite after cone calorimeter flame test indicates a mineral composition of forsterite (Mg_2SiO_4) and aluminum silicate (Al_2O_3, SiO_2). It can be concluded that the char layer of ablative nanocomposite is a ceramic based on aluminum silicate.

5. Conclusions

1. The polymer layered silicate nanocomposites result in an improvement in thermal stability compared with the composite counterpart. A relatively tough, inorganic ceramic layer forms during thermal degradation of the nanocomposites. This refractory ceramic results in at least an order of magnitude decrease in the mass loss rate relative to the composite, even for as little as 6 wt.% exfoliated layered silicate.
2. The NKA3 nanocomposite has a 35% lower HRR and 22% lower mass loss than the asbestos cloth/phenolic composite.
3. The improvement in ablation performance of these nanocomposites relative to the net polymer or traditional filled systems with a comparable inorganic fraction could be associated to the ceramic forming in the nanocomposites char layer. The base of this ceramic layer is aluminum silicate that protected the ablation char layer against the thermal erosion effects. This nanoscopic morphology is comparable to the length scale of the decomposition and ceramic forming reactions determined by the temperature profile and the diffusivities of the reactants and products. Thus, a uniform supply of inorganic precursor to the ceramic is always available during the decomposition process.
4. In 9×10^6 W/m K external conventional heat flux condition, ablation performance of NKA3 nanocomposite is 43.4% higher than the asbestos cloth/phenolic composite.

Acknowledgement

The authors would like to acknowledge the bodies to support this work.

References

[1] H.S. Shen, J.J. Zheng, X.L. Huang, Dynamic response of shear deformable laminated plates under thermomechanical loading and resting on elastic foundations, Compos. Struct. 60 (2003) 57–66.
[2] A.P. Mouritz, Post fire flexural properties of fibre reinforced polyester, Epoxy and Phenolic Composites, J. Mater. Sci. 37 (2002) 1377–1386.
[3] J. Kim, W. Lee, S.W. Tsai, Modeling of mechanical property degradation by short term aging at high temperatures, Compos.: Part B 33 (2002) 531–543.
[4] Y.I. Dimitrienko, Thermo-mechanical behaviour of composite materials and structures under high temperatures: 1-materials, Compos.: Part A 28 (1997) 453–461.
[5] L. Torre, J.M. Kenny, A.M. Maffezzoli, Degradation behaviour of a composite material for thermal protection systems, part 1- experimental characterization, J. Mater. Sci. 33 (1998) 3137–3143.
[6] D Cho, B. Yoon, Microstructural interpretation of the effect of various matrices on the ablation properties of carbon fiber reinforced composite, Compos. Sci. Technol. 61 (2001) 271–280.
[7] J. Staggs, Simple mathematical models of char forming polymers, Polym. Int. 49 (2000) 1147–1152.
[8] M.R.E. Looyeh, A. Samanta, S. Jihan, J. McConnachie, Modeling of reinforced polymer composites subject to thermo-mechanical loading, Int. J. Numer. Methods Eng. 63 (2005) 898–925.
[9] R.A. Vaia, G. Price, P.N. Ruth, H.T. Nguyen, J. Lichtenhan, Polymer/layered silicate nanocomposites as high performance ablative materials, Appl. Clay Sci. 15 (1999) 67–92.
[10] T. Kashiwagi, R.H. Harris, X. Zhang, R.M. Briber, B.H. Cipriano, S.R. Raghavan, W.H. Awad, J.R. Shields, Flame retardant mechanism of polyamide 6-clay nanocomposites, Polymer 45 (2004) 881–891.
[11] J.K. Pandey, K.R. Reddy, A.P. Kumar, R.P. Singh, An overview on the degradability of polymer nanocomposites, Polym. Degrad. Stab. 88 (2005) 234–250.
[12] N. Sheng, M.C. Boyce, D.M. Parks, G.C. Rutledge, J.I. Abes, R.E. Cohen, Multiscale micromechanical modeling of polymer/clay nanocomposites and the effective clay particle, Polymer 45 (2004) 487–506.
[13] R.L. Frost, S.J. Gaast, M. Zbik, J.T. Kloprogge, G.N. Paroz, Birdwood kaolinite: a highly ordered kaolinite that is difficult to intercalate-an XRD, SEM and Ramman spectroscopic study, Appl. Clay Sci. 20 (2002) 177–187.
[14] Kaolinite mineral data, 2002, http://www.Mindat.Org/min-2156.html.
[15] J.L. Capitaneo, F.T. Silva, V.R. Caffarena, Aluminosilicate nanocomposite material, Appl. Mineral. 1 (2004) 45–48.
[16] J.L. Capitaneo, F.T. Silva, V.R. Caffarena, Preparation of layered polyvinyl chloride (PVC)-kaolinite nanocomposite, Appl. Mineral. 1 (2004) 53–56.
[17] Y. Komori, Y. Sugahara, K. Kuroda, Intercalation of alkylamines and water into kaolinite with methanol kaolinite as an intermediate, Appl. Clay Sci. 15 (1999) 241–252.
[18] C.T. Johnston, G. Sposito, D.F. Bocian, R.R. Birge, Vibrational spectroscopic study of the interlamellar kaolinite-dimethyl sulfoxide complex, J. Phys. Chem. 88 (1984) 5959–5964.
[19] A.R. Bahramian, M. Kokabi, M.H.N. Famili, M.H. Beheshty, Ablation and thermal degradation behaviour of a composite based on resol type phenolic resin; process modeling and experimental, Polymer 47 (2006) 3661–3673.
[20] Y.I. Dimitrienko, Thermo-mechanical behaviour of composites under local intense heating by irradiation, Compos.: Part A 31 (2000) 589–599.

[21] R.E. Lyon, Pyrolysis kinetics of char forming polymers, Polym. Degrad. Stab. 61 (1998) 201–210.
[22] M.H. Yang, The thermal degradation of acrylonitrile-butadiene-styrene terpolymer under various gas conditions, Polym. Test. 19 (2000) 105–110.
[23] Determination of kinetic parameters for thermal decomposition of phenolic ablative materials by multiple heating rate method, Naval Surface Weapons Center (N43) Dahlgren, VA 22448 (1990).
[24] L.P. Kanevce, G.H. Kanevce, Z.Z. Angelevski, Comparison of two kinds of experiments for estimation of thermal properties of ablative composite, in: 3rd International Conference on Inverse Problems in Engineering, Port Ludlow, WA, USA, 1999, June 13–18.
[25] M.S. Chetan, R.S. Ghadage, R. Rajan, V.G. Gunjikar, S. Ponrathnam, Thermolysis of orthonovolaks.II. phenol-formaldehyde and (-naphthol-formaldehyde resins, J. Appl. Polym. Sci. 50 (1993) 685–692.